

RESEARCH

Open Access



# Comparative study of electron temperature and ion energy in two different magnetic nozzle thruster designs

Clara E. Schäfer<sup>1\*</sup>, Jens Schmidt<sup>1</sup>, Felix Plettenberg<sup>1</sup>, Yung-An Chan<sup>1</sup>, Martin Grabe<sup>1</sup>, Jan Martinez Schramm<sup>1</sup>, Kristof Holste<sup>2</sup> and Peter J. Klar<sup>2</sup>

\*Correspondence:  
clara.schaefer@dlr.de

<sup>1</sup>Spacecraft Department,  
German Aerospace Center,  
37073 Göttingen, Germany

<sup>2</sup>Institute of Experimental  
Physics I, Justus Liebig University,  
35392 Giessen, Germany

## Abstract

Conventional ion thruster technologies face challenges such as electrode and grid erosion and the need for additional neutralizer devices. In this article, we discuss two thruster concepts that achieve plasma acceleration by means of a magnetic nozzle, and thus avoid the need of a neutralizer device. The concept of a magnetic nozzle converting the thermal energy available in the electrons movement to ion kinetic energy is a well accepted model in the community. We discuss a novel thruster concept based on electrode-less electron cyclotron resonance plasma generation via a slot antenna design. The geometry of this thruster concept results in a converging-diverging character of the magnetic field topology along the plume direction. To this date it is not known in which way this new thruster design influences the electron dynamics and thus the ion energy. To understand the correlation between ion energy and electron temperature of this thruster system, it is compared with a well-known thruster prototype operating on similar principles, however, realizing microwave coupling and magnetic field topology in a different way. Both thruster designs operate within comparable power, frequency, and volume flow ranges. The ion energy with maximum probability is measured for both thrusters using a retarding potential analyzer in the same vacuum environment. Additionally, the electron temperature is measured with a Langmuir probe for various operation points of the thrusters, differing in input power level, volume flow, set excitation frequency, and argon or xenon as propellant.

## Introduction

Electrode-less plasma thrusters with magnetic nozzles (MN) offer high operational flexibility and longer lifetimes. They are of great interest for long-distance space travel and become prominent in recent thruster development [1]. Resembling the traditional “e Laval” nozzle, a MN typically possesses a divergent magnetic field structure caused by an applied magnetic field. The divergent field guides and accelerates a magnetized plasma jet into vacuum [2]. The diverging magnetic field radially confines the plasma and helps the conversion of perpendicular into parallel kinetic energy of the plasma particles. The ambipolar electric field, converts the thermal energy motion of the electrons into ion

kinetic energy. Therefore the electron dynamics plays a crucial role in configuring the ambipolar electrostatic field in the plume, responsible for ion acceleration and ultimately thrust generation [1]. One advantage of this approach to plasma acceleration is the absence of a direct contact between the plasma and the structure walls. This reduces wall losses. Moreover, no electrodes are required for plasma acceleration or neutralization. Instead, the MN utilizes the expanding electron gas to neutralize the ion beam without the need for additional cathode installation [1]. This extends the thruster's lifetime and eliminates the need for complex neutralizer devices. Additionally, the capability to use a multitude of different propellants is advantageous, along with the scalability and adaptability of a MN [2]. Various thrusters, both established and under development, exhibit different characteristics from the perspective of plasma generation and heating, yet they all realize the physics of quasi-neutral, quasi-collisionless plasma expansion in a MN [1].

In the following, we discuss the thruster concept DEEVA (*DLR Electrode-less ECR Via microwave plasma Accelerator*), which allows electrode-less plasma generation by microwaves, fulfilling the electron cyclotron resonance (ECR) condition [3]. Plasma acceleration is achieved by the diverging magnetic field of a MN. This thruster concept is compared with a prototype of the well-known thruster concept developed by the Office national d'études et de recherches aérospatiales under the project *Magnetic Nozzle Electron Cyclotron Resonance Thruster* (MINOTOR) [4–8]. While both thruster concepts employ a MN, are of similar size, and are designed to operate within a similar frequency and power range, they differ in terms of the approach for microwave coupling into the plasma. This design difference also results in different magnetic field topology requirements. The microwave coupling in case of MINOTOR is achieved by a coaxial coupling structure, where the inner conductor is directly exposed to the plasma. The overall aim of the DEEVA development is to create a fully electrodeless thruster that eliminates the need for an inner electrode. Without exposed inner conductors, grids, or similar components, the design avoids sputtering effects and performance degradation over time, which is expected to extend the DEEVA thruster's operational lifetime [9]. The DEEVA thruster concept realizes electrode-less coupling by an annular waveguide (ring cavity) defined by two resonant coupling slots into the plasma discharge chamber made of quartz. The idea of using such a slot antenna (SLAN) for a thruster is based on the work by Korcz et al. [10].

In recent years, several studies have explored the connection between electron temperature and ion energy, and have addressed the effect of electron cooling on ion energy by making use of the polytropic expansion law [1, 11–13]. As it is reported in literature, a constant ratio value of electron temperature and ion energy, describing the polytropic index, was determined. The resulting ratios were described in dependence on magnetic field strength. Experimental findings have shown relatively stable ratios of electron temperature to ion energy across a wide range of parameters. However, while polytropic models offer simplicity and approximate the effects of electron cooling, their accuracy in describing plasma expansion processes has been questioned by theoretical studies [12, 13]. A comprehensive understanding of the relationship between electron dynamics and heat flux/ion energy in expanding plasma systems remains elusive for the relatively new DEEVA thruster. The question, whether we also observe a constant ratio between electron temperature and ion energy provides the motivation for this research. Investigating

the effect of changing operational parameters - such as varying input power, frequency settings, and volume flow of propellant - on the correlation between electron temperature and ion energy is essential. Comparing the DEEVA and the MINOTOR prototype under the same operating conditions (e.g. same vacuum chamber, similar background pressures, same diagnostic tools) allows us to carry out detailed studies of the impact of the microwave coupling method and magnetic field topology on plasma parameters. In particular we vary the operation conditions of the thrusters and conduct retarding potential analyzer (RPA) as well as Langmuir probe (LP) measurements for a determination of electron temperature and ion energy. Preliminary studies showed that the determined electron temperatures and ion energies in case of the DEEVA thruster are higher, when performing with argon as propellant instead of xenon. Therefore, the discussed operational changes in the following comprises varying propellant (xenon and argon), varying input power, changing excitation frequency set and variable volume flow.

## Methods and experimental set up

### Test facility and set up

The experiments are conducted at the DLR in Göttingen in the vacuum facility *Simulationsanlage für Treibstrahlen Göttingen - Miniatur Triebwerke* (STG-MT). The chamber has a length of 1 m and a diameter of 1.1 m. It is equipped with two backing pumps, a rotary vane pump and a roots pump yielding a base pressure of  $10^{-3}$  mbar. For lower pressure ranges a turbomolecular pump is added achieving pressure values down to  $10^{-6}$  mbar and background pressures during thruster operation in the range of 2 to  $8 \times 10^{-5}$  mbar. For the operation of the thrusters, we use the microwave signal generator KU-SG 2.45-250A of the company Kuhne Electronics GmbH as well as the Bronkhorst mass control unit (MCU) for maximum 50 sccm air. For the reported experiments the MCU is calibrated inhouse for xenon and argon with a fine-weight scale. It has to be mentioned that in the following we use the term 'input power' to describe the power emitted by the microwave generator. For upcoming experiments, a bi-directional coupler or a vector network analyzer will be used to determine the power depleted in the plasma. Therefore, with the term 'input power' we refer to the forward sent power, with a given uncertainty to what degree the forward sent power is actually coupled into the plasma. The gases in use are xenon and argon. The mapping of each thruster is performed as follows: For all operation points the plasma parameters are measured with LP in  $d = 100 \pm 0.5$  mm distance to the thruster exit. The ion energy is investigated by means of RPA measurements at the same distance. Multiple measurements at the same thruster setting are performed and yield the experimental uncertainty of the results. The set up can be seen in Fig. 1.

### Thrusters under investigation

The operating principle of both ECR thrusters with MN is the ionization of the propellant via ECR and the acceleration by a divergent magnetic field [5, 14, 15]. Schematic images of the thrusters can be seen in Fig. 2. In presence of a magnetic field, charged particles (electrons and ions) are trapped along the magnetic field lines in such a way that they are circulating (gyrating) around the field lines, due to Lorentz forces [15]. Since electrons are much lighter than ions, their movement about the magnetic field

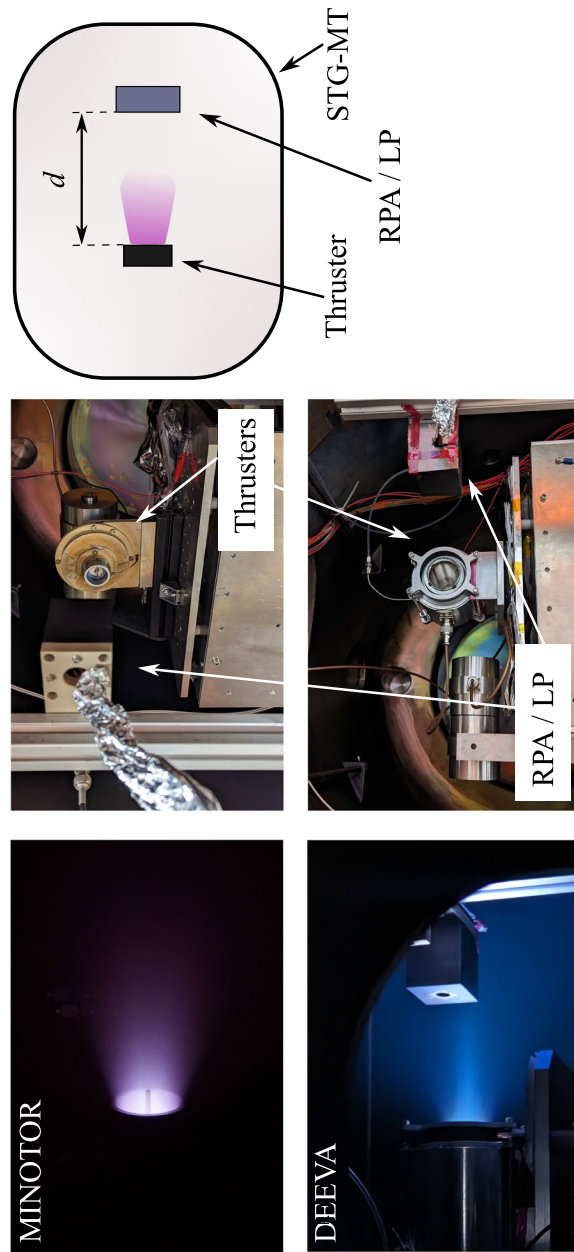


**Fig. 1** Test set up of the MINOTOR and DEEVA prototype and diagnostics in the vacuum chamber STG-MT. On the top row, one can see MINOTOR, on the bottom the DEEVA prototype is pictured. The left column shows the running thrusters and their beams, the right column depicts the test set up, with the thrusters, as well as the diagnostic tools, the retarding potential analyzer (RPA) and the Langmuir probe (LP). On the right hand side, one can see the top view of the test set up. With the thruster on the left and the diagnostics in a distance  $d = 100$  mm from the thrusters exit plane

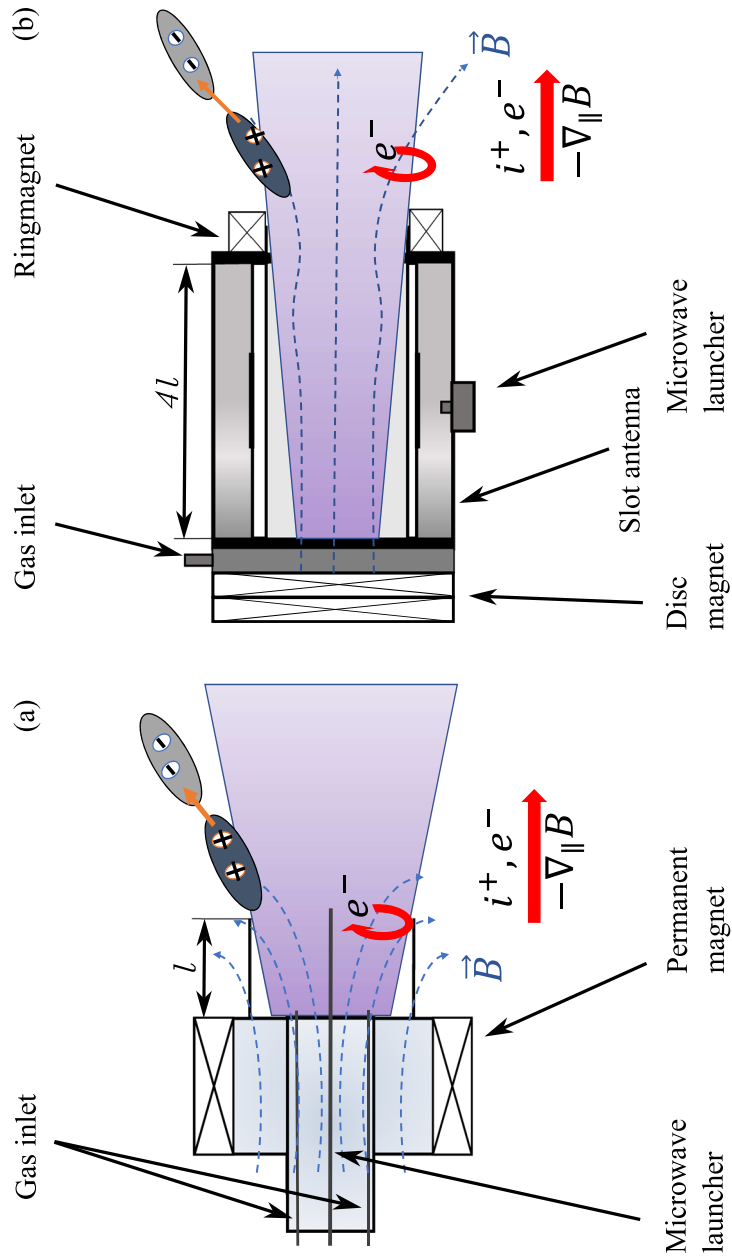


**Fig. 2** Schemes of the ECR thrusters. MINOTOR (a) is pictured on the left, the thruster is pictured in black. The magnetic field lines are pictured in blue, and the particle motions are pictured in red.  $e^-$  are the electrons and  $i^+$  are the ions. As for DEEVA (b) on the right: The slotted antenna (consisting of two cylinders and the slots), the quartz tube and the gas inlet is indicated. Here the magnetic field lines are also pictured in blue, and the particle motions are pictured in red. For both thrusters the ambipolar electric field is indicated in orange. Additionally for both thrusters the microwave launchers are depicted. The length  $l \approx 20$  mm serves as a size orientation, however the drawings are not to scale

lines is decisive for the behavior of a magnetized plasma [15]. Additionally to the gyration about the field lines, a parallel motion of the guiding center is superimposed, if a velocity component parallel to the magnetic field lines is present [14, 15]. The angular frequency of the electrons around the field lines is given by the cyclotron frequency. If an electromagnetic wave with that cyclotron frequency is applied, the electron is resonantly accelerated by the electric field of the wave. It absorbs the energy of the electromagnetic wave, gains kinetic energy and increases the impact ionization process rate [14, 15]. This ECR zone takes the form of a plane, where the resonant excitation conditions of a magnetic field strength of 87.5 mT and the microwave frequency of 2.45 GHz are met (compare Fig. 3).

The acceleration of the produced ions is assumed to originate from two processes: First, the faster reaction of the electrons to density disturbances or density gradients, due to their lower mass [15, 16]. The pressure gradient between the thruster interior and the environment leads to the faster response of electrons in comparison to the heavier ions [15]. As a result of the charge separation an ambipolar electric field forms, leading to the acceleration of the ions towards the negative space charge [15]. The second driving mechanism is the gradient in the magnetic field. Due to the inhomogeneity of the magnetic field parallel to the magnetic field lines, the magnetic moment  $\mu$  of the charged particles (forming due to the gyration of the particles about the magnetic field lines) and the mass of the particle  $m$ , can be used to formulate an acceleration ( $\dot{v}_{||}$ ) opposite to the gradient direction  $\nabla_{||}B$  [15, 17]:

$$m\dot{v}_{||} = -\mu\nabla_{||}B. \quad (1)$$

This force can cause particles to reflect in the converging sections of a MN. This phenomenon, known as the magnetic mirror effect, has been the subject of investigation in several recent studies aimed at modeling MN behavior [1, 2, 13, 18]. Depending on the magnetic field ratio (the ratio of maximum field strength to minimum field strength,  $\frac{B_0}{B_{\max}}$ ), a critical pitch angle  $\alpha$  leading to particle reflection can be determined [15]:

$$\sin \alpha > \sqrt{\frac{B_0}{B_{\max}}}. \quad (2)$$

The pitch angle is defined by the parallel and orthogonal velocity components of the particle ( $\tan \alpha = \frac{v_{\perp}}{v_{||}}$ ). Thus, in a convergent-divergent MN, the axial motion of individual ions or electrons is governed by both electrostatic and magnetic mirror forces [1]. While the electrostatic field accelerates ions and decelerates electrons axially in the convergent and divergent MN regions, the magnetic mirror force decelerates both ions and electrons in the convergent part and accelerates them axially in the divergent part.

The dimensions of the MINOTOR thruster are motivated by the wavelength of the microwave excitation chosen, therefore, optimized for 2.45 GHz [19]. The inner diameter of the thruster is given as 27 mm and an antenna made out of stainless steel of 20 mm length, serving as a long semi-open coaxial coupling structure [19]. The close end of the coaxial structure used to feed the microwave into the thruster is a boron nitride plate. The static and divergent magnetic field is created by an annular permanent magnet consisting of a Nd-Fe-B alloy [19, 20]. The electromagnetic wave is fed to the inner

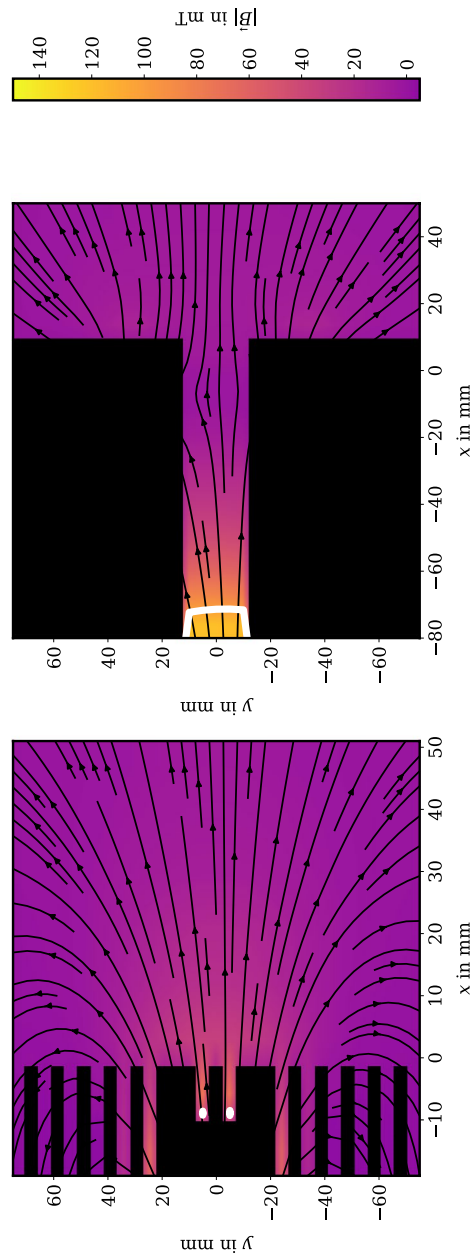


**Fig. 3** Magnetic field topology of the thruster prototypes in the  $x, y$  plane. On the left are the measured results of the MINOTOR prototype, on the right are the magnetic field strengths of the DEEVA prototype. The black masks mark the part of the prototypes inaccessible to the Hall probe.  $x = 0$  marks the position of the downstream plane of the ring magnet and in case of MINOTOR the tip of the inner conductor - ergo the thruster exit plane. As for  $y = 0$  marks the centerline of the thruster. The colourmap depicts the strength of the magnetic field, while the streamline vectors depict the magnetic field lines in  $x$  and  $y$  direction. Additionally the equipotential line of 87.5 mT is shown as a white line, marking the ECR zone at a set microwave frequency of 2.45 GHz

conductor of the thruster via a coaxial to waveguide to coaxial transition. The two hollow cylinders have a length of 100 mm, respectively. The connection to the coaxial cable from the microwave generator is a copper antenna reaching inside the waveguide with a length of 27 mm. A second antenna of the same length is then placed in a 100 mm distance plus a slit of roughly 2 mm size in between the two cylinders in order to receive the microwave signal and irradiate inside the thruster. This assembly enables microwave coupling without mechanical or electrical contact. This way a thruster floating potential can be measured at the conducting parts, and accurate thrust balance measurements could be performed [19]. One statement omnipresent in former studies on the ECR thruster MINOTOR is the operation of the thruster in floating mode. As it is stated in literature, observations indicate that the thruster potential depends on the electron temperature and is directly proportional to the ion energy [20, 21]. During our measurement campaign both prototypes are operated in grounded mode.

The other thruster under investigation is the DEEVA prototype thruster, shown in Fig. 2 on the right. In the slot antenna (SLAN), the microwave power is coupled from an annual waveguide (ring cavity) by two resonant coupling slots into the plasma discharge chamber made of quartz. The SLAN is made of aluminum. It consists of two cylinders which act as waveguides. The microwave enters the bigger cylinder via a N-type 14 mm long launcher made of copper. As a result, modes develop between the inner and outer waveguide. Under certain conditions, e.g. when the two slots are at a certain angle to the launcher, 45° in this work, the microwave is fed into the inner part of the inner cylinder. Backplates are mounted on both ends of the two cylinders. A ring magnet with a remanence of 400 mT is positioned on the downstream end. Upstream, two disc magnets, each with a remanence of 1400 mT are applied. The magnets are oriented in an attracting manner, the polarizations therefore show in the same direction. Typical microwave power ranges for ignition and operation lay between 10 and 100 W. The gas is introduced into the quartztube with an inner diameter of 45 mm via an in-house designed gas inlet. The gas inlet consists of two parallel plates, one with 12 holes. The gas is fed into the space between the two plates and is distributed over the entire diameter through the holes.

A comparison of the measured magnetic field topologies of the both thruster prototypes in the  $x, y$  plane can be seen in Fig. 3. The spatial magnetic field distributions of the prototypes are measured in three spatial directions using a 3D Hall probe from the company Projekt Elektronik GmbH. The probe is placed on three linear stages, so that the magnetic field can be also mapped in three dimensions inside and outside the prototype's body. The range of the probe in use is  $\pm 200$  mT and the linearity error is given as  $\pm 0.1$  mT. In Fig. 3 the color map represents the strength of the magnetic field (the absolute value based on  $B_x, B_y, B_z$ ), while the streamlines depict the magnetic field lines in the  $x$  and  $y$  directions (i.e.,  $B_x, B_y$ ). The black masks indicate the parts of the prototypes inaccessible to the Hall probe. The line  $x = 0$  marks the downstream plane of the ring magnet, and in the case of the MINOTOR, the tip of the inner conductor-this is referred to as the thruster exit plane for all the prototypes. This plane represents the wall-free region of the thruster system, where the beam can expand without wall losses. The line  $y = 0$  marks the centerline of the thruster. To indicate where the ECR condition is met for the frequency of 2.45 GHz (requiring a field strength of 87.5 mT), white lines are used

to show the ECR zone. These white lines represent the equipotential line at 87.5 mT. For the MINOTOR thruster, the ECR condition is met right at the back wall of the thruster. Additionally, the strictly diverging nature of the magnetic field lines supports the direct acceleration of the quasi-neutral plasma. For the DEEVA prototype, the ECR condition is met on the upstream part of the SLAN, extending across the entire diameter of the quartzglas tube. The magnetic field lines exhibit a slight asymmetry, which could be due to probe misalignment with the magnets or changes in the magnets' properties after extended operation. Nonetheless, the field lines show a diverging pattern towards the thruster exit plane. After a small converging section immediately following the thruster exit at  $x = 0$ , the magnetic field becomes strictly divergent.

As reported in Lafleur et al. [11], stronger magnetic fields result in smaller ion energy to temperature ratios, according to a non-Maxwellian kinetic model and Faraday probe measurements. Additionally, it was concluded that the magnetic field does not cause additional ion acceleration in the downstream region of the nozzle, as evidenced by the fact that ion energy values will remain high even if the magnetic field is turned off [11]. However they also stress that stronger magnetic fields lead to better confinement conditions and less wall losses. In these studies, the ratio of electron temperature to ion energy often exhibited a rather constant value. Specifically, in the absence of a magnetic nozzle, a ratio of 7 was observed, while stronger magnetic fields led to a ratio of about 4. Ion energies were measured in the range of 100 eV, with electron temperatures exceeding 20 eV [11]. However, it is important to note that while the ECR thruster design studied by Lafleur et al. bears resemblance to the MINOTOR prototype examined in our study, the entire thruster setup has undergone changes during the development, regarding geometry and performance. For example, in the previous study, the magnetic field was generated by coils, allowing a control of magnetic field strength, while the MINOTOR prototype in our case is equipped with permanent magnets.

### Langmuir probe evaluation

One of the most technically simple, yet difficult to interpret, diagnostics tools is the Langmuir probe (LP)[15]. This probe consists of one, two or three conductive electrodes of various shapes, directly brought into the plasma. If a single electrode probe is introduced into the plasma and the voltage  $U$  is varied with respect to a reference potential, a plasma characteristic current signal  $I$  can be measured [22]. By analyzing this current-voltage characteristic it is possible to capture properties of the plasma, such as temperatures, potentials, densities etc [15]. The extraction of these plasma parameters requires an appropriate theory. We apply the Druyvestein method for the single Langmuir probe measurement [23, 24]. Using that we determine directly the EEDF ( $f(E)$ ) based on the second derivative of the measured current voltage characteristic  $\frac{d^2 I_e}{dU^2}$ , the probe surface  $A_p$ , the electron mass  $m_e$  and charge  $e$  and the energy  $E$  of the electron impinging on the probe:

$$f(E) = \frac{2}{e^2 A_p} \sqrt{2m_e E} \frac{d^2 I_e}{dE^2}. \quad (3)$$

It should be noted that here we use a cylindrical probe with a surface of  $A_p = 31.4 \pm 0.5 \text{ mm}^2$ . We correct the measured current  $I_0$  by subtracting the linear

fitted ion current  $I_i$  to obtain the second derivative of the electron current  $I_e = I_0 - I_i$ . Taking the moment of the distribution function yields the electron temperature  $T_e$  of the plasma:

$$T_e = \frac{2}{3n_e} \int_0^\infty f(E) E dE. \quad (4)$$

An exemplary evaluation procedure and determination of the EEDF can be seen in Fig. 4. We point out that this model assumes an isotropy of the plasma which is a crude approximation.

We have to state, that the conversion of the electrons movement into the ion kinetic energy happens in close vicinity to the thruster. Since we are measuring at a distance of 100 mm the electrons should have cooled down already at the measurement position. However, the chosen position for the Langmuir probe is primarily determined by practical constraints. While it would be ideal to measure plasma parameters closer to - or probably inside - the source, several factors limit our ability to do so. First, the DEEVA thruster has geometric restrictions that prevent probe insertion into the discharge vessel, unlike the MINOTOR prototype, which has a more accessible structure. Additionally, DEEVA's sensitivity to coupling conditions often hinders thruster ignition when objects are placed too close to the source. Invasive measurement methods, like the Langmuir probe, also tend to disturb plasma parameters near the thruster's exit plane. Another aspect is the orientation of the probe in stronger magnetic fields (ergo closer to the prototypes): According to Lobbia et al. [23] an anisotropic effect on the electron current collection is mitigated when the anisotropic drifting beam component is parallel to the electrode surface. Furthermore it is stated in Lobbia et al. [23] that the effect of magnetic fields can be neglected in the limit of the probe radius being much smaller than the local Larmor radius, which is for our plasma most likely the case. Former studies regarding these contradictory recommendations (measuring parallel and orthogonal to the magnetic field lines, compare Fig. 2) lead to the decision to measure in parallel orientation [25]. A strong anisotropy and non-Maxwellian behavior of the EEDF was observed for the MINOTOR prototype [25]. Those measurements were carried out closer to the thruster, about 60 mm [25]. Preliminary measurements regarding the relevance of the distance of the probe to the thruster allowed us to conclude that, at a greater distance, like 100 mm, the orientation of the probe in relation to the magnetic field lines plays a negligible role. In addition, the non-Maxwellian character of the plasma could not be confirmed at that distance which is explained by the smaller magnetic field strength in greater distance to the thruster. Therefore, we choose a probe distance of 100 mm to minimize these influencing effects, drawing comparisons to similar studies, such as those by Lafleur and Correyero [8, 11], where the probe was placed at distances comparable to our experimental set up.

While electron temperature and plasma potential near the source are, of course, crucial for ion acceleration, our study focuses on comparing the ratios of plasma parameters between two prototypes using the same measurement methods and detector positions for both thrusters. A detailed spatial mapping of plasma parameters is planned for future studies but is beyond the scope of this article.

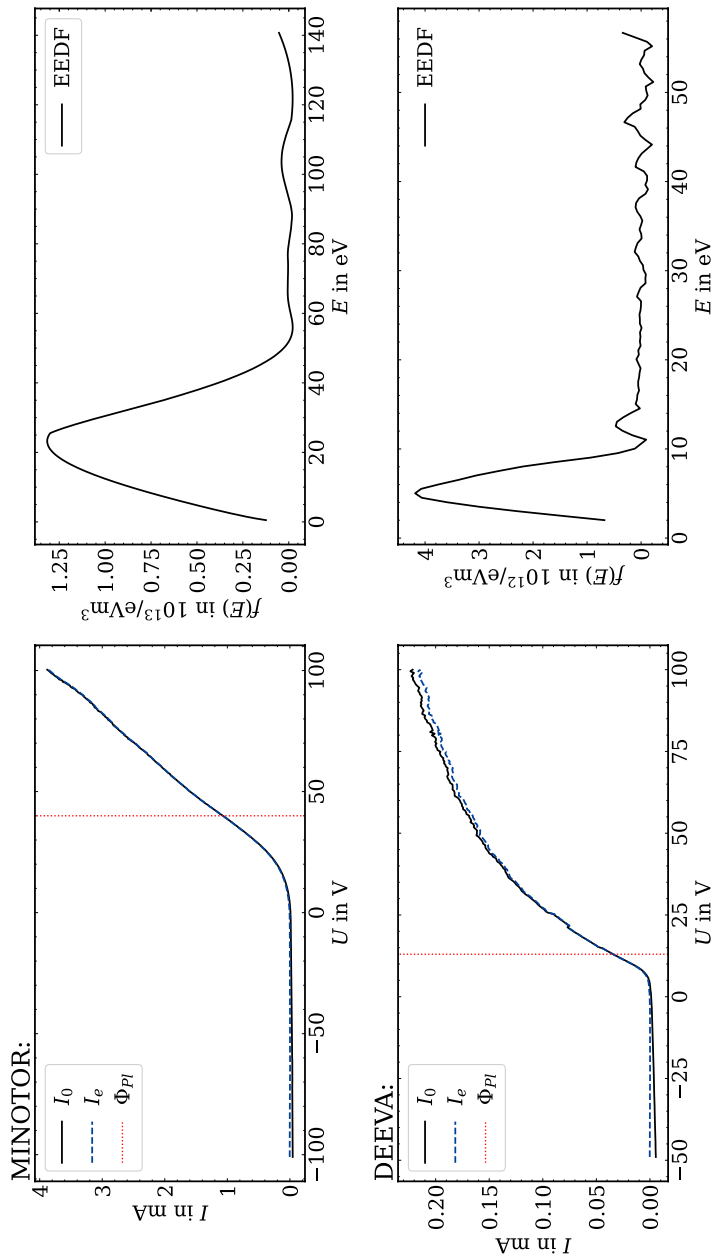


**Fig. 4** Exemplary evaluation of Langmuir probe data. The data of the MINOTOR prototype can be seen in the top row, at operation conditions 1 sccm of xenon, 30 W input power, and frequency set of 2.45 GHz. The DEEVA thruster can be seen on the bottom, at 1 sccm of argon, 30 W input power, and frequency set of 2.45 GHz. On the left the current-voltage characteristic  $I_0$  can be seen. After subtracting the ion saturation current the resulting electron current  $I_e$  is depicted in blue. The vertical red line depicts the determined plasma potential  $\Phi_{PI}$ . In the MINOTOR case, the plasma potential is 42 V, in the DEEVA case it is 12 V. On the right, one can see the determined electron-energy distribution functions  $f(E)$  of the two prototypes which show in both cases a single Maxwellian character

### Retarding potential analyzer evaluation

A challenge arises when trying to extract information about the ion distribution function with a Langmuir probe, which operates at a positive potential, repelling ions, and draws electron-saturation current [26]. This electron saturation current is typically significant enough to overshadow any variations in the ion current that might provide insight into the ion temperature or energy distribution [26]. Therefore, more sophisticated analyzers, such as the “ridded energy analyzer” so called, retarding potential analyzers (RPAs) are often employed to obtain information about the ion energy distribution functions of plasmas. These devices consist of a system of grids at different potentials [26, 27]. An exemplary evaluation procedure can be seen in Fig. 5. Be advised that we are showing sections of the spectrum as a demonstration. The measurement procedure includes a scan of the spectrum from 0 to 200 V to identify the drop in the raw current measurement. Afterwards several measurements with a higher resolution of up to 0.1 V are performed, from which standard deviations of the most probable ion energies can be determined. Examples of these high-resolution measurements are shown in Fig. 5. As one can see, the measured current value of the MINOTOR prototype

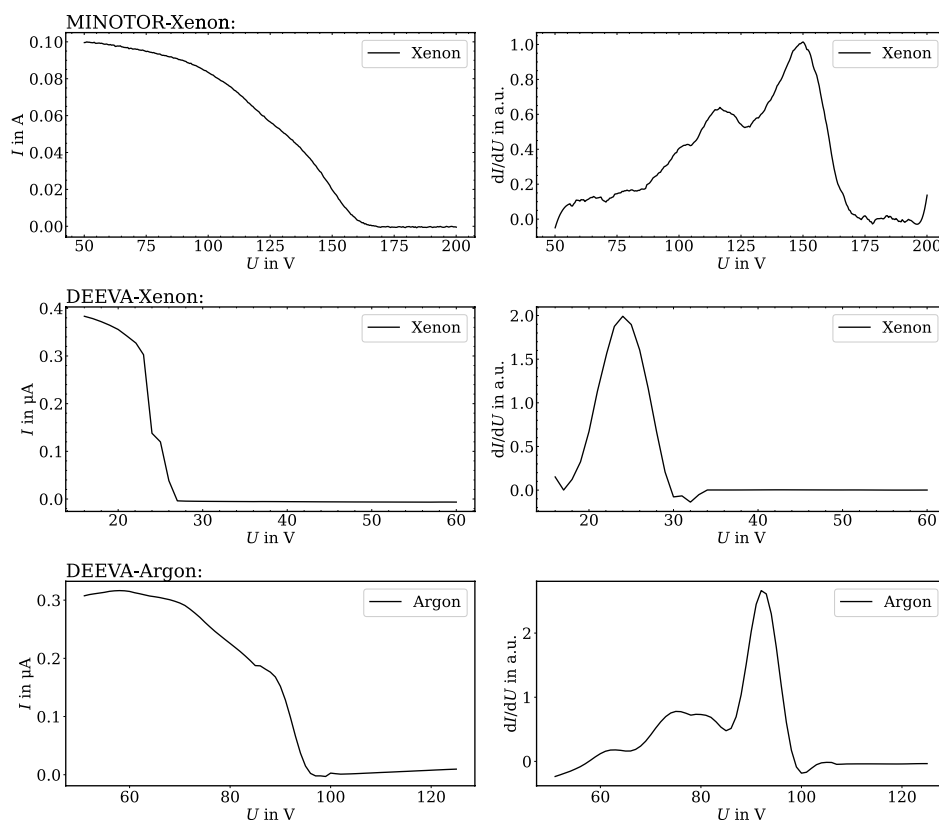


**Fig. 5** Exemplary evaluation of RPA data. The data of the MINOTOR prototype can be seen in the top row, at operation conditions 1 sccm of xenon, 30 W input power, and frequency set of 2.45 GHz. The center row depicts the data of the operation of DEEVA with xenon as propellant at 1 sccm, 30 W input power, and frequency set of 2.45 GHz. The operation of the DEEVA thruster with argon can be seen on the bottom row, at 1 sccm, 30 W input power, and frequency set of 2.45 GHz. On the left the current-voltage characteristic of the RPA can be seen. On the right the first derivative of the raw current measurement  $dI/dU$ , the IEDF, can be seen. The ion energy with the highest probability determined in this case for MINOTOR is approximately 150 eV, in the DEEVA case it is for xenon about 25 eV and for argon around 95 eV

exceeds the current of the plume of the DEEVA thruster by a factor of  $10^6$ . This shows that there is much more ion current exiting the MINOTOR prototype than there is for the DEEVA thruster. However, since we cannot estimate the effect of additional charge densities existing between the grids (which can change the potential and therefore influence current measurements [26]), hence a quantitative determination of the ion density in the beam is not possible with this set up. Therefore, we focus on determining the ion energy with the maximum probability and the ion energy distribution function (IEDF). The latter is determined by the first derivative of the measured current, the maximum of this distribution function is then the most probable ion energy  $E_{i,max}$ . For both thrusters we determine a broadened, bi-Maxwellian IEDF. The RPA used is a commercial four gridded RPA from the company Plasma Controls, LLC. It has an entrance aperture of 12.7 mm and an overall transparency of 35 %. For the operation, a picoammeter from Keithley with a resolution of 1 nA in the 2 mA range is employed. The electron retarding grid, as well as the secondary electron grid is held at  $-40$  V. The first grid is kept floating and the floating potential is measured with a commercial Voltcraft multimeter (VC870).

### Experimental results

As depicted in Figs. 5 and 6, the maximum ion energies determined for the DEEVA thruster are significantly higher when argon is used as the propellant instead of xenon. Despite identical thruster operational parameters - namely, same power, frequency, and volume flow rates - operation with argon yields multiple times higher maximum energies than operation with xenon. We measure ion energies up to 140 eV in case of operation with argon, while the operation with xenon leads to ion energies not exceeding 30 eV. Importantly, the magnetic field topology is the same in both cases. Furthermore, it can be noted, that the electron temperature of the DEEVA thruster operated with xenon is not exceeding 2 eV over all parameter changes. Moreover, discernible trends can be observed from the parameter variations. In the left-hand plot of Fig. 6, we see that the ion energy with the highest probability also increases with increasing power at a frequency set to 2.45 GHz and a volume flow of 1 sccm argon. For xenon, by comparison, the change in the determined ion energy seems to be negligible at the same power and volume flow setting. The same holds for the frequency variation at power input of 30 W and a volume flow of 1 sccm. While in case of argon a maximum ion energy can be detected at about the design frequency, the xenon curve seems to be independent of frequency variation. A clear decrease in ion energy can be seen with increasing volume flow of argon at constant frequency 2.45 GHz and input power of 30 W, while in comparison the performance with xenon hardly changes.

As it is described before, the correlation of electron temperature and ion energy is a main driving force in a magnetic nozzle design. We can follow in the footsteps of previous research by comparing the trends and ratios of the two plasma parameter, electron temperature and ion energy with the highest probability. A simple comparison of the trends can be seen in Fig. 7. The left plot shows the electron temperature  $T_e$  and the ion energy with the maximum probability  $E_{i,max}$  determined in case of MINOTOR as a function of volume flow of xenon. With increased volume flow, the electron temperature, as well as the ion energy decreases. This is in accordance with observations reported in

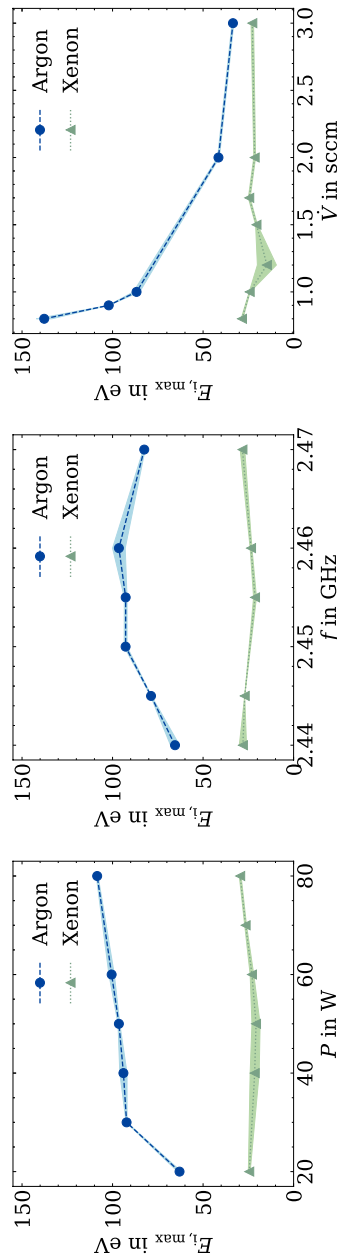


**Fig. 6** Ion energies with maximum probability determined of the DEEVA thruster operated with xenon and argon as propellant. The plot on the left shows power variations at a frequency set of 2.45 GHz and a volume flow of 1 sccm of argon (dashed line) and xenon (dotted line). The center plot depicts frequency variation at power input of 30 W and a volume flow of 1 sccm. The right hand side plot shows the volume flow variation at the constant frequency 2.45 GHz and input power of 30 W. The filled space shows the standard deviation of the resulting values from multiple measurements

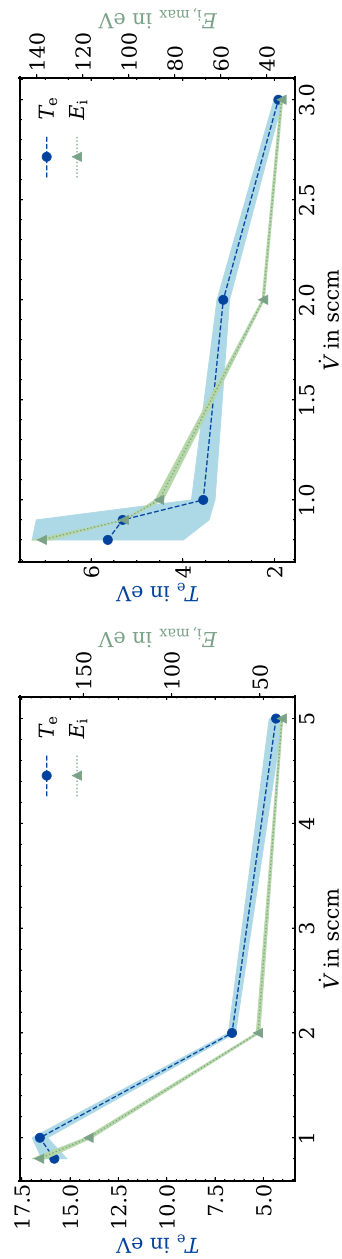


**Fig. 7** Correlation of electron temperature and ion energy for MINOTOR on the left and DEEVA on the right at variable volume flow settings. MINOTOR is operated at 2.45 GHz and input power of 30 W, the volume flow of xenon is varied. DEEVA on the right, is operated at 2.45 GHz and input power of 30 W, and the volume flow of argon is varied. The electron temperature  $T_e$  can be seen in blue and its scale can be seen on the left. The ion energy with the highest probability  $E_{i,max}$  can be seen in green, with the scale on the right. The filled space shows the standard deviation of the resulting values from multiple measurements

literature for the MINOTOR prototype. The same trends can be seen in the right plot for the DEEVA thruster operated at different volume flows of argon. Both thrusters are kept at 2.45 GHz and input power of 30 W.

In Fig. 8 the ratio of electron temperature and ion energy  $E_i/T_e$  for variable thruster operational settings can be seen for the DEEVA and the MINOTOR prototype. The ratio for the MINOTOR prototype is plotted in blue and that for the DEEVA prototype in green. The plot on the left shows the dependence on power variations at a frequency set of 2.45 GHz and a volume flow of 1 sccm of argon (in case of DEEVA) and xenon (in case of MINOTOR). The center plot depicts the dependence on frequency variation at power input of 30 W and a volume flow of 1 sccm. The right plot shows the dependence on volume propellant flow (of argon, in case of DEEVA; and xenon, in case of MINOTOR) at the constant frequency 2.45 GHz and input power of 30 W. As one can see the resulting ratio in case of MINOTOR in blue is quite constant at a value of about 11 over all operational points. DEEVA in green shows a good correlation in dependence on power at a ratio of 19. However, in case of frequency and volume flow dependence, the correlation is not as constant as for MINOTOR case. Over all three operation parameter variations the ratio of electron temperature to ion energy in case of MINOTOR is about 10 for xenon as propellant, while for DEEVA the ratio is in the range of 20 for argon as propellant.

## Conclusion

We compared two ECR thruster prototypes with MN, MINOTOR and DEEVA, under comparable operating conditions and employing the same diagnostic methods. The plasma parameters and the ion energy distribution were characterized with LP and RPA respectively.

First and foremost, it is important to note that the LP and RPA are positioned in proximity to the thruster. This proximity significantly influences the thruster's performance and the plasma parameters obtained. Despite the LP being oriented parallel to the magnetic field lines, which theoretically should enable the measurement of bi-Maxwellian shaped EEDFs, in most of the cases our observations reveal Maxwellian-shaped distribution functions for both thrusters, as shown in Fig. 4. However, given our primary interest in electron temperature in this study, employing double Langmuir probe measurements could serve as an effective means to validate the results presented here.

Additionally, it is important to note that the testing chamber STG-MT is of medium size, which can potentially have a negative impact on the thruster's performance due to limitations in pumping speed. It is well established that higher background pressures result in a decrease in the mean free path lengths of plasma particles. Consequently, the decrease in ion energy and electron temperature observed for both the DEEVA and MINOTOR prototypes with increasing volume flow may be attributed to this phenomenon. Moreover, this could also contribute to the broadening of the ion energy distribution functions, as illustrated in Fig. 5.

The significant disparity in electron temperature and ion energy observed during DEEVA operation with argon versus xenon, as shown in Figs. 5 and 6, warrants further investigation. Currently, there is no conclusive theory to explain this phenomenon. We observe an overall better performance with argon as a propellant regarding

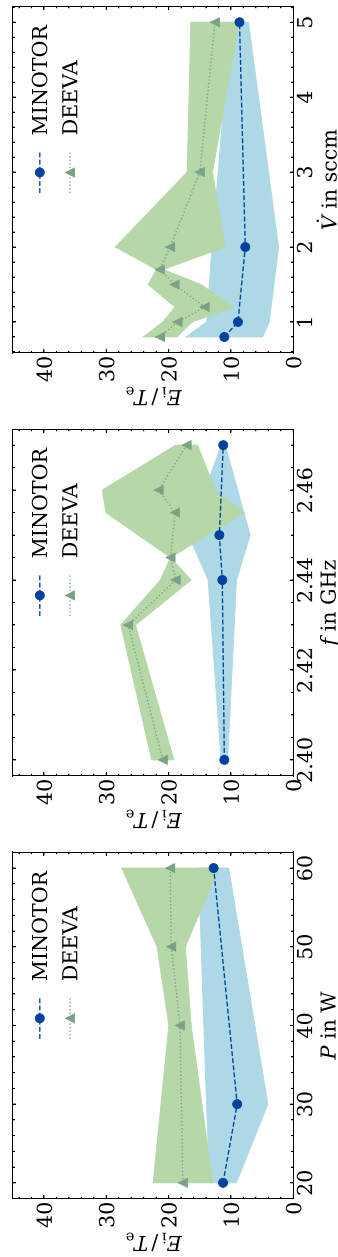


**Fig. 8** Ratio of electron temperature and ion energy for variable thruster operational settings. The ratio of ion energy with the highest probability and electron temperature  $E_i/T_e$  can be seen for both thrusters at variable input power, frequency and volume flow set. The MINOTOR prototype's ratio can be seen in blue, the DEEVA thruster's can be seen in green. The plot on the left shows power variations at a frequency set of 2.45 GHz and a volume flow of 1 sccm of argon (in case of DEEVA) and xenon (in case of MINOTOR). The middle plot depicts frequency variation at power input of 30 W and a volume flow of 1 sccm. The right plot shows the volume flow variation (of again argon, in case of DEEVA; and xenon, in case of MINOTOR) at the constant frequency 2.45 GHz and input power of 30 W. The filled space shows the standard deviation of the resulting values from multiple measurements

electron temperature and ion energy. These results have been reproduced on multiple occasions and seem to be a characteristic of the new DEEVA thruster. In contrast, literature indicates that MINOTOR prototypes exhibit different behavior when operated with argon. Specifically, the overall performance, including ion energy, ion current, specific impulse, and thrust, is not as good with argon as it is with xenon [28]. Since the setup and operational points remain unchanged when switching gases for our investigations on the DEEVA thruster, the only variable affecting thruster performance is the type of gas used. The observed differences can be therefore solely attributed to the differences in gas mass, the cross section for electron collisions, or/and ionization energy (15.76 eV for argon compared to 12.13 eV for xenon).

In existing literature, a constant ratio between electron temperature and ion energy has often been observed. For instance, in the absence of a MN, a ratio of approximately 7 was reported, while stronger magnetic fields led to a ratio of 4 [11]. We note a similar constant ratio in the case of the MINOTOR prototype, albeit with a ratio more than twice as high as previously reported values. This discrepancy can be attributed to higher electron temperatures reported in the literature, where measurements exceeding 20 eV were recorded alongside similar or smaller ion energies, as determined in our case [11]. Understanding the variance between the results of the ECR thruster prototype in literature and our observations is challenging. Factors such as the thruster setup (including magnetic field and topology, microwave generator, cabling, and mass flow control unit), LP position, data acquisition and evaluation methods, ion energy detection method, and facility effects (e.g., chamber size, pumping rates); all play significant roles in determining plasma parameters and performance. For example, the prototype in Lafleur et al. [11] employed magnetic field coils, allowing the current in the coils to be adjusted to achieve wished field strengths inside the source. These set up differences motivated our analysis on comparing the here described MINOTOR and DEEVA prototypes, both examined under identical conditions in the same vacuum chamber, with consistent background pressures, thruster setups, and diagnostic tools and methods. Our findings reveal a relatively constant ratio of electron temperature to ion energy in the MINOTOR case, suggesting that expansion is predominantly driven by electron dynamics, with higher electron temperatures resulting in higher ion energies. The DEEVA thruster operated with argon demonstrates a stable ratio in dependence on power variations and a relatively constant ratio of about 20 in case of frequency and volume flow variations. This can be attributed to comparable ion energies to MINOTOR (up to 150 eV) but significantly lower electron temperatures, not exceeding 12 eV. Since the electron temperature within the source and therefore the electron dynamics in the expanding MN region are unknown, assessing how the reported ratios are affected by variations in magnetic field topologies, strengths, and microwave coupling mechanisms requires the development of an analytical model specific to the DEEVA thruster. Additionally, non-intrusive diagnostic methods are essential for determining plasma properties within the discharge tube and gaining insight into the cooling processes.

#### **Acknowledgements**

Many thanks to the ONERA team for providing the MINOTOR prototype for the comparison measurements. Furthermore, warmest thanks to the ion thrusters research group at JLU for their tremendous effort and support during the preparatory measurement campaigns.

**Open Access**

I confirm that I understand *Journal of Electric Propulsion* is an open access journal that levies an article processing charge per article accepted for publication. By submitting my article I agree to pay this charge in full if my article is accepted for publication.

**Dual Publication**

The results/data/figures in this manuscript have not been published elsewhere, nor are they under consideration (from you or one of your Contributing Authors) by another publisher.

**Authorship**

I have read the Nature Portfolio journal policies on author responsibilities and submit this manuscript in accordance with those policies.

**Third Party Material**

All of the material is owned by the authors and/or no permissions are required

**Authors' contributions**

C.E.S. performed the measurements, analysis of the data and wrote the manuscript. J.S. and F.P. designed, built, and pre-tested the thruster. Y.A.C. designed the Langmuir probe in use. M.G. and J.M.S. advised on the measurement campaign and provided the test facility/test opportunities. K.H. and P.K. supervised the work, advised on the measurement campaign, and provided facilities and measurement possibilities during preliminary measurements. All authors revised the manuscript and approved the version to be published.

**Funding**

Open Access funding enabled and organized by Projekt DEAL. This work was exclusively funded by DLR (Deutsches Zentrum für Luft- und Raumfahrt).

**Data availability**

No, I do not have any research data outside the submitted manuscript file.

**Declarations****Competing Interests**

No, I declare that the authors have no competing interests as defined by Springer, or other interests that might be perceived to influence the results and/or discussion reported in this paper.

Received: 22 July 2024 Accepted: 2 December 2024

Published online: 10 December 2024

**References**

- Kim J, Chung KJ, Takahashi K, Merino M, Ahedo E (2022) Kinetic electron cooling in magnetic nozzle: Experiments and modeling. *Plasma Sources Sci Technol* 32(7):073001
- Merino M, Ahedo E (2017) Magnetic nozzles for space plasma thrusters. *Encycl Plasma Technol* 2:1329–1351
- Schmidt J, Simon J, Grabe M (2022) The deep thruster concept. In: 37th International Electric Propulsion Conference. Electric Rocket Propulsion Society, Boston
- Vialis T, Jarrige J, Packan D (2017) Geometry optimization and effect of gas propellant in an electron cyclotron resonance plasma thruster. In: Proc. 35th Int. Electr. Propuls. Conf. Electric Rocket Propulsion Society. pp 1–12
- Packan D, Elias P, Jarrige J, Vialis T, Correyero S, Peterschmitt S, Porto J, Merino M, Sánchez-Villar A, Ahedo E, et al (2019) H2020 minotor: Magnetic nozzle electron cyclotron resonance thruster. In: 36th International Electric Propulsion Conference. Electric Rocket Propulsion Society
- Correyero S, Merino M, Elias PQ, Jarrige J, Packan D, Ahedo E (2019) Characterization of diamagnetism inside an ECR thruster with a diamagnetic loop. *Phys Plasmas* 26(5):053511
- Correyero Plaza S, Jarrige J, Packan D, Ahedo Galilea E (2017) Measurement of anisotropic plasma properties along the magnetic nozzle expansion of an electron cyclotron resonance thruster. In: 35th International Electric Propulsion Conference (IEPC). Electric Rocket Propulsion Society
- Correyero S, Jarrige J, Packan D, Ahedo E (2019) Plasma beam characterization along the magnetic nozzle of an ECR thruster. *Plasma Sources Sci Technol* 28(9):095004
- Schmidt J, Schaefer C, Chan YA, Plettenberg M F und Grabe (2024) Development and testing of a microwave-heated plasma thruster. In: 38th International Electric Propulsion Conference IEPC 2024. Electric Rocket Propulsion Society
- Korzec D, Werner F, Winter R, Engemann J (1996) Scaling of microwave slot antenna (slan): a concept for efficient plasma generation. *Plasma Sources Sci Technol* 5(2):216
- Lafleur T, Cannat F, Jarrige J, Elias P, Packan D (2015) Electron dynamics and ion acceleration in expanding-plasma thrusters. *Plasma Sources Sci Technol* 24(6):065013
- Merino M, Ahedo E (2014) Influence of electron and ion thermodynamics on the magnetic nozzle plasma expansion. *IEEE Trans Plasma Sci* 43(1):244–251
- Martinez-Sanchez M, Navarro-Cavallé J, Ahedo E (2015) Electron cooling and finite potential drop in a magnetized plasma expansion. *Phys Plasmas* 22(5):053501
- Goebel D, Katz I (2008) *Fundamentals of electric propulsion: ion and Hall thrusters*, vol 1., John Wiley & Sons, Hoboken

15. Stroth U (2011) *Plasmaphysik*. Springer, Berlin
16. Fridman A, Kennedy L (2004) *Plasma physics and engineering*. CRC Press, Boca Raton
17. Longmier B, Bering E, Carter M, Cassady L, Chancery W, Díaz FC, Glover T, Hershkovitz N, Ilin A, McCaskill G et al (2011) Ambipolar ion acceleration in an expanding magnetic nozzle. *Plasma Sources Sci Technol* 20(1):015007
18. Merino M, Nuez J, Ahedo E (2021) Fluid-kinetic model of a propulsive magnetic nozzle. *Plasma Sources Sci Technol* 30(11):115006
19. Peterschmitt S (2020) Development of a stable and efficient electron cyclotron resonance thruster with magnetic nozzle. PhD thesis, Institut polytechnique de Paris
20. Vialis T, Jarrige J, Aanesland A, Packan D (2018) Direct thrust measurement of an electron cyclotron resonance plasma thruster. *J Propuls Power* 34(5):1323–1333
21. Cannat F, Lafleur T, Jarrige J, Chabert P, Elias PQ, Packan D (2015) Optimization of a coaxial electron cyclotron resonance plasma thruster with an analytical model. *Phys Plasmas* 22(5):053503
22. Demidov V, Ratynskaia S, Rypdal K (2002) Electric probes for plasmas: The link between theory and instrument. *Rev Sci Instrum* 73(10):3409–3439
23. Lobbia R, Beal B (2017) Recommended practice for use of langmuir probes in electric propulsion testing. *J Propuls Power* 33(3):566–581
24. Druyvesteyn M (1930) Der niedervoltbogen. *Z Phys* 64(11):781–798
25. Schäfer C, Zorn J, Holste K, Klar P (2023) Influences on langmuir probe measurements by an ecr thruster with magnetic nozzle. *New Results Numer Exp Fluid Mech XIV* 154:153–162
26. Hutchinson I (2002) Principles of plasma diagnostics. *Plasma Phys Control Fusion* 44(12):2603
27. Lai S, Miller C (2020) Retarding potential analyzer: Principles, designs, and space applications. *AIP Adv* 10(9):095324
28. Jarrige J, Elias PQ, Cannat F, Packan D (2013) Performance comparison of an ecr plasma thruster using argon and xenon as propellant gas. In: *Proceedings of the 33rd International Electric Propulsion Conference*. pp 2013–420. Electric Rocket Propulsion Society

### **Publisher's Note**

Springer Nature remains neutral with regard to jurisdictional claims in published maps and institutional affiliations.